DOI: 10.21062/mft.2025.041 http://www.journalmt.com

Process Prediction and Force Measurement of Hot Rolling Process for 6061 Aluminum Alloy Wire

Jinn-Jong Sheu (0000-0001-6959-1580), En-Hsuan Chien (0009-0000-6551-4318)
Department of Mold and Die Engineering, National Kaohsiung University of Science and Technology. No. 415, Jiangong Rd., Sanmin Dist., Kaohsiung City, Taiwan. E-mail: jjsheu@nkust.edu.tw; enhsuanchien@gmail.com

This study examines the two-pass hot rolling process of 6061 aluminum alloy wire, focusing on forming load measurement to evaluate process stability and its effects on dimensional accuracy and mechanical property uniformity. Using response surface methodology (RSM), process parameters and forming loads were analyzed to assess their influence on mechanical property distribution and verify the applicability of load measurement in process quality evaluation. A full-factorial finite element simulation was conducted to investigate the effects of pre-forming section reduction rate, material temperature, roll speed, and friction coefficient. Experimental results indicate that forming load measurements effectively capture variations in initial wire temperature and reveal the influence of material velocity and roll speed. Load data also identify the spike phenomenon caused by improper roll positioning, leading to abnormal load surges and reduced mechanical property uniformity. The strong agreement between experimental forming loads and FEM simulations validates the reliability of the proposed measurement method. This study provides a basis for wire rolling process design and machine learning-based quality prediction, supporting advancements in smart manufacturing applications.

Keywords: Two pass wire rolling, Bézier curve groove-shape design, Aluminum alloy 6061

1 Introduction

1.1 Rolling Process and Load Distribution Optimization

Compared to wire drawing, wire rolling offers significant advantages in reducing material damage and improving surface quality, making it particularly suitable for high-strength applications [1]. By designing appropriate roll groove shapes, the distribution of rolling load and shear force can be optimized, thereby improving material flow and surface quality [2]. Numerous studies have investigated roll groove design strategies for achieving more uniform load distribution, minimizing forming load variation, and enhancing the dimensional accuracy of the final product [6,11,21-27].

Aksenov et al. [3] conducted numerical simulations to examine the effects of different groove designs on rolling load, discovering that adjusting roll gaps effectively optimizes load distribution. Lambiase [4] applied artificial neural networks (ANNs) to predict geometric changes during rolling and combined genetic algorithms (GA) to optimize roll gap and groove design, achieving a more uniform load distribution. Minutolo et al. [5] proposed a new groove design and experimentally verified that it significantly reduces forming loads and improves the geometric accuracy of the final product. Additionally, Sheu et al. [6] studied the Bézier curve groove roll design method, comparing it with the traditional round-oval-round design and found that the Bézier curve groove enables higher compression ratios per pass, thereby enhancing forming efficiency.

Regarding load distribution and stress control, Overhagen et al. [7] introduced a three-roll rolling model, demonstrating that the three-roll system reduces rolling loads, minimizes slippage, and improves material flow stability. Chenot et al. [8] applied finite element analysis to simulate hot rolling processes, confirming that controlling rolling loads can effectively regulate material flow and final geometry, ensuring product dimensional accuracy and stability. Byon et al. [9,10] experimentally investigated the effects of roll gap and wear on forming loads and geometric precision, concluding that improper gap adjustment and roll wear lead to non-uniform forming loads, negatively impacting the dimensional accuracy of the final product.

1.2 Rolling Load Measurement

In hot rolling processes, non-uniform load distribution can lead to localized material flow anomalies, causing a sudden increase in forming loads, which subsequently affects the uniformity of mechanical properties. Rolling load monitoring, as addressed in this study, has been the focus of several research efforts.

Kim et al. [11] developed a knowledge-based expert system, integrating finite element analysis and empirical formulas to optimize roll groove design for

round and square bars, thereby improving load uniformity. Lambiase et al. [12] employed finite element analysis and optimization algorithms to establish an automated rolling design method, demonstrating that this approach reduces design time and improves the dimensional stability of the final product. Li et al. [13] explored the impact of roll damage on load distribution, finding that damage models effectively predict roll lifespan and optimize roll design to minimize geometric variations in the final product.

1.3 Application of Sensor Technology in Rolling Load Monitoring

The application of load sensor technology in metal forming processes has been extensively studied, with many researchers exploring methods to improve sensor accuracy and enhance the reliability of load monitoring data in process control.

Groche et al. [14] compared different sensor installation positions and measurement methods in stamping processes, revealing that embedding sensors within the die provides more detailed load information, facilitating process control and quality management. Kim et al. [15] developed a bolt-type piezoelectric sensor to monitor die and process conditions in forging, demonstrating that the sensor effectively detects tool wear and process variations, thereby extending die lifespan and optimizing production processes.

For intelligent monitoring of rolling processes, Traub et al. [16] proposed a Decision Support System (DSS) that analyzes sensor data to reduce operator dependency and enhance rolling process stability. Traub et al. [17] further explored the integration of sensors and automated decision-making systems in rolling, finding that real-time load measurement effectively identifies inefficiencies and incorrect process settings, thereby reducing reliance on human expertise and improving process automation.

Therefore, this study aims to evaluate the feasibility and effectiveness of using forming load measurements as indicators for process quality assessment in the hot rolling of EN AW-6061-T6 aluminum alloy wire. To achieve this, a series of experiments were conducted to analyze the effects of wire temperature, pre-forming reduction rate (hR_n), and roll positioning on forming load behavior and strain distribution. By comparing measured load data with FEM simulations and mechanical testing, this study seeks to verify the potential of forming load signals for supporting process adjustment and defect detection in practical rolling applications. The findings are expected to provide a foundation for enhancing quality evaluation and enabling future integration with smart manufacturing systems.

2 Wire Rolling process and Roller design

2.1 Roller groove design

In the wire rolling process, rolls are used to gradually reduce the wire diameter until the target size is achieved. Compared to the conventional wire drawing process, rolling significantly reduces surface friction due to its rolling contact mechanism. This experiment adopts a typical round-oval-round groove configuration, where the oval groove is designed using the Bézier curve method (Fig. 1) [6]. A wire with an initial outer diameter of 20 mm is rolled down to 16 mm through two rolling passes, with an area reduction rate (AR_n) of 10% per pass, totaling 20% across both passes.

In the first pass, a Bézier curve-designed oval groove is used to roll the wire into an elliptical cross-section with a short axis of 14.6 mm, corresponding to a section reduction rate (hR_n) of 27%. In the second pass, a round groove is used to further roll the wire into a circular cross-section with a final outer diameter of 16 mm.

$$AR_n = (A_n - A_{n-1})/(A_{n-1}) \quad (1)$$

$$hR_n = (h_n - h_{n-1})/(h_{n-1}) \quad (2)$$

Where:

A_n, A_{n-1}…The cross-sectional areas of the wire in the n -th and (n − 1)-th passes, respectively, while AR_n is the area reduction rate for the n -th pass.

h_n, h_{n-1}…The section reductions in the n -th and (n − 1)-th passes, and hR_n is the section reduction rate for the n -th pass (Fig. 2).

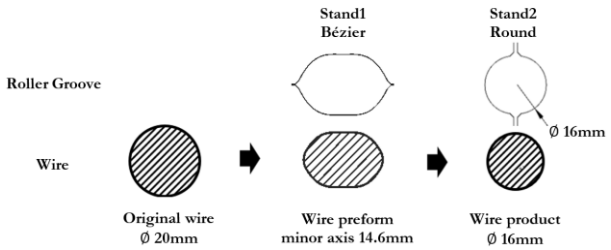

Fig. 1 *Roller groove-shape designs for round-Bézier-round*

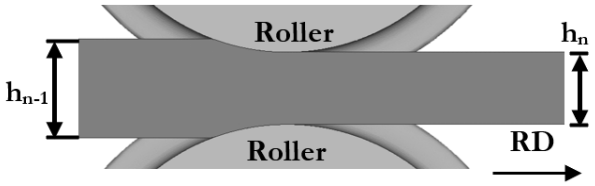

Fig. 2 *Section reduction rate*

2.2 Experimental conditions

In the rolling experiment setup, the first pass functions as the pre-forming pass, while the second pass serves as the final round-shaped forming pass. The roll axes of the two passes are oriented at a

90-degree angle to each other, enabling the wire to undergo reduction forming in two different directions (Fig. 3). Each roll consists of two grooves of the same type but different sizes. During the rolling process, only one side of the groove is engaged in forming, referred to as the "rolling side", while the non-forming side is referred to as the "empty side".

The primary factors influencing the geometry of the final product in the second pass are the short-axis deformation in the first-pass oval groove and the adjustment of the roll gap [9]. Based on the initially designed 27% hR_n, this study further simulates poor roll adjustment conditions by modifying the roll gap, setting the hR_n to 24%. During the hot rolling process, EN AW-6061-T6 aluminum alloy is heated above its recrystallization temperature of 250°C [19]. The wire heating temperature significantly impacts energy consumption and forming load on the equipment. Therefore, this study designs two temperature conditions for comparison: 400°C and 350°C, the latter representing a scenario with reduced heating time.

Three sets of forming experimental parameters were designed, as shown in Tab. 1. The comparison between Case 1 and Case 2 is used to analyze the effect of wire temperature on the forming load, while the comparison between Case 1 and Case A investigates the influence of hR_n on the forming load. Additionally, the study observes changes in the forming load in Stand 2 when a spike phenomenon occurs due to the reduced hR_n in Stand 1.

Tab. 1 *Forming Experiment Cases*

Experimental Parameters	Case1	Case2	CaseA
Stand1 hR_n	27%	27%	24%
Wire Temperature	400° C	350° C	400° C

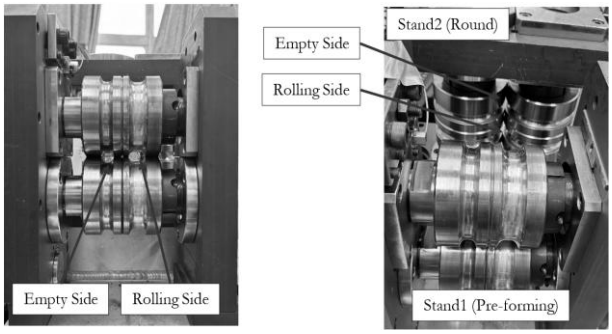

Fig. 3 *Wire rolling rollers and installation*

2.3 FEM Simulation of the Wire Rolling Process

This study employs Simufact Forming to perform finite element method (FEM) simulation of wire rolling, aiming to verify whether different experimental parameters influence forming geometry and forming load. The symmetric boundary conditions are illustrated in Fig. 4. The material used is EN AW-6061-T6 aluminum alloy, modeled as a perfectly plastic material, as detailed in Tab. 2.

The roll speed ratio for the first and second passes is set at 2.00:2.52, with an initial roll temperature of 20°C and a shear friction coefficient between 0.5 and 0.8 (Friction Correction Curve at 400 Degrees, Fig. 5). In the simulation, the rolls are considered rigid bodies, while the wire is modeled with 1/4 symmetry. The wire mesh consists of hexahedral elements with a size of 0.5 mm, determined through a convergence test. The FEM parameters are listed in Tab. 3 and Tab. 4.

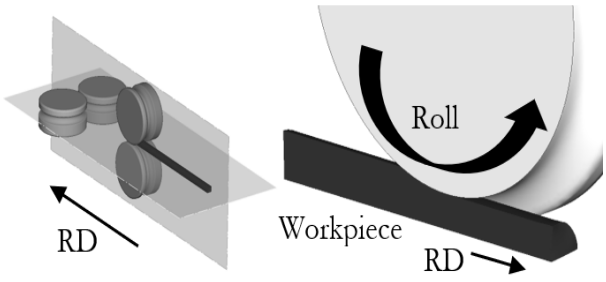

Fig. 4 *Simulation Model and Symmetry plan*

Tab. 2 *EN AW-6061-T6 aluminum alloy Material Flow stress (MPa) Model*

Strain rate	Wire Temperature 300 °C	Wire Temperature 400 °C	Wire Temperature 500 °C
0.1	130	60	38
1.0	160	80	42

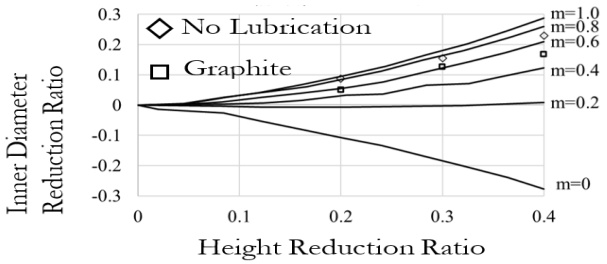

Fig. 5 *EN AW-6061-T6 aluminum alloy, Friction Correction Curve at 400°C*

Tab. 3 *Simulation parameters*

Process Conditions	Values
Initial wire diameter (mm)	20
Initial wire length (mm)	200
Maximum roll diameter (mm)	100
Element type	Hexahedral
Element size(mm)	0.5

2.4 Virtual Mechanical Properties Dataset

This study utilizes FEM to establish a dataset containing process parameters, wire mechanical properties, and forming loads, and applies response surface methodology (RSM) to predict the quality of mechanical property distribution. This dataset enables an analysis of the correlations between process parameters, forming loads, and final product quality, and also allows for a comparison between simulated forming loads and experimental data. The process parameter combinations used in the dataset are detailed in Tab. 4.

In the first pass (oval pre-forming), the hR_n is a critical factor influencing the final circular cross-section of the wire [9]. Additionally, in the hot rolling process, the strain rate significantly affects material deformation behavior. Therefore, the roll speed is set between 25–75 rpm, covering the typical speed range for rolling processes. Friction influences whether natural rolling occurs, and based on the friction correction experiment (Fig. 5), the constant shear friction coefficient is set between 0.5–0.8, while the material temperature is varied between 300–400°C.

This study adopts equivalent strain [18] as a reference metric for quality evaluation, and the strain difference between the wire's outer surface (Y_a) and center (C) (Fig. 6) is used as an indicator of mechanical property uniformity.

Tab. 4 *Establishment of virtual mechanical property parameters in rolling process*

Level	Roller speed (RPM)	Stand1 hR_n (%)	Wire Temperature(°C)	Friction (-)
1	25.0, 31.5	27	300	0.5
2	50.0, 62.9	24	350	0.6
3	75.0, 94.4	22	400	0.7
4		19		0.8

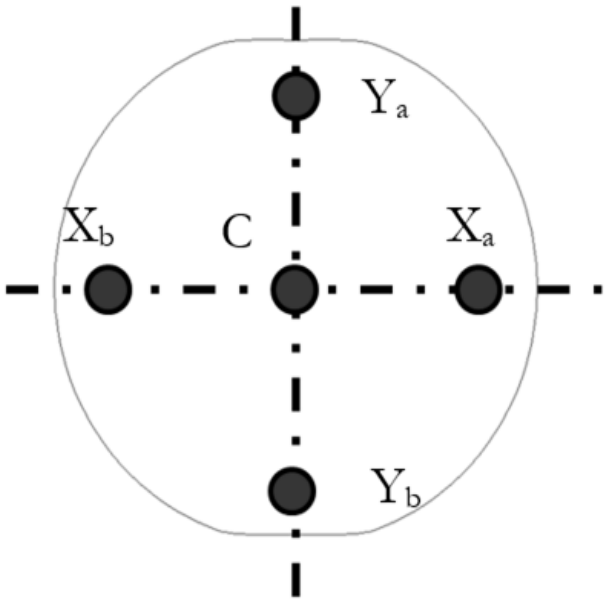

Fig. 6 *Measurement of strain on the outside (Y) and center (C) of the wire*

3 Sensor and measurement system

To capture the characteristic signals of forming loads during the rolling process, this study installs load sensors in the rolling equipment and designs an integrated mechanism that combines sensor preloading with roll position adjustment (Fig. 7). This mechanism utilizes a wedge-type bearing seat pressure plate to adjust the bearing seat (roll) position, forming a wedge relationship between the bearing seat pressure plate and the sensor pressure plate to achieve both sensor preloading and locking. The adjustment process consists of two steps: first, the bearing seat pressure plate is used to position the rolls, and then, the sensor pressure plate is adjusted to set the sensor's preloading force, ensuring that the preloading force remains consistent after roll positioning.

This study considers the load capacity of the sensor and evaluates its mechanical behavior under different loading conditions. Additionally, the effect of sensor installation position (Fig. 8) on its sensitivity to

forming load response is analyzed. A sensor position evaluation fixture is designed, and a sensitivity experiment is conducted. The experiment involves varying the installation position conditions by modifying the thickness ratio (D/H) Fig. 9) and applying a 5-ton universal testing machine to simulate rolling loads acting on the sensor fixture. Based on the experimental results (Fig. 10), it is confirmed that the sensor output voltage is influenced by changes in D/H. The most sensitive installation distance (D/H = 0.1) is selected as the optimal sensor installation position in the rolling mill. The force sensor used in this study was the WFS model developed by the Industrial Technology Research Institute (ITRI), Taiwan.

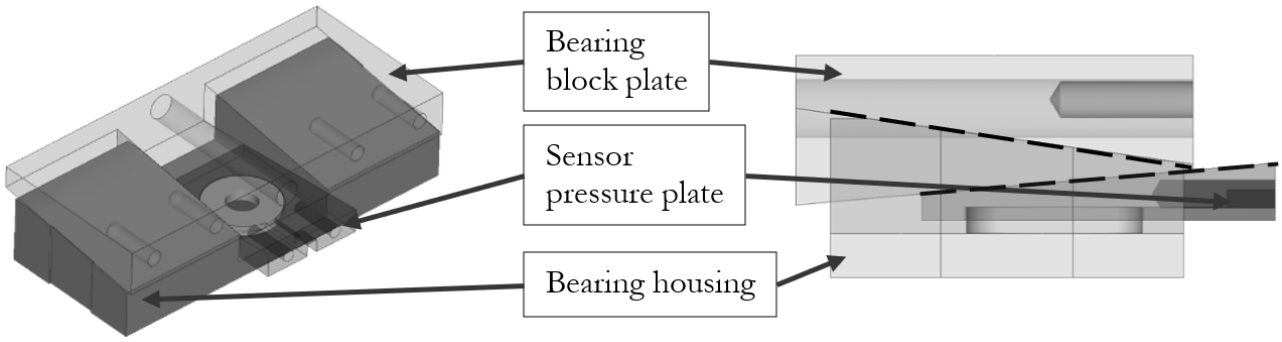

Fig. 7 *Integration design of load sensor preload mechanism and roll adjustment mechanism*

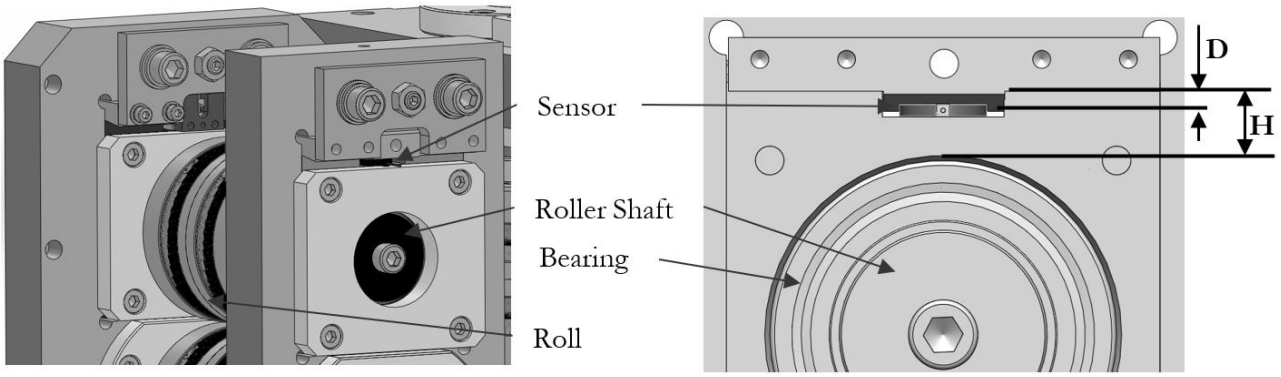

Fig. 8 *The sensor installation position on the rolling mill (with certain components concealed)*

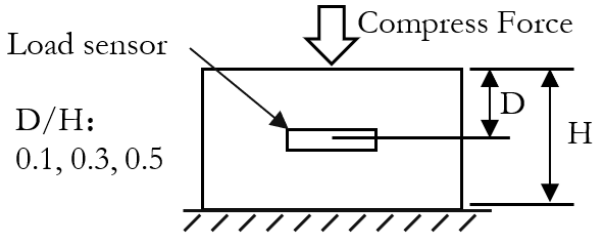

Fig. 9 *Sensor Position Evaluation Experimental Fixture*

In this study, the sensor module (Fig. 7) is designed and installed on the upper roll of the rolling mill stand, with the installation position set at D/H = 0.1 (Fig. 8). Using roll positioning and sensor preloading techniques, the sensor is preloaded to 1V after roll positioning, and the output voltage baseline is reset to zero to ensure uniform sensor preloading across all sensors.

The rolling equipment, module system, and display interface after sensor installation are shown in Fig. 11. This system collects sensor voltage signals and displays real-time forming voltage variations on a machine-side screen. Additionally, by establishing a voltage-to-load conversion relationship through compression experiments, the voltage signals are converted into forming loads.

In this study, the first and second passes are denoted as S1 and S2, respectively, where the rolling side is referred to as R, and the empty side is referred to as L.

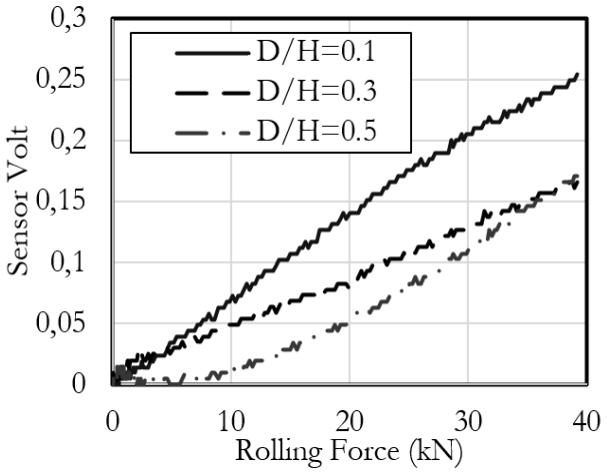

Fig. 10 *The relationship between sensor output voltage and rolling force varies with changes in D/H*

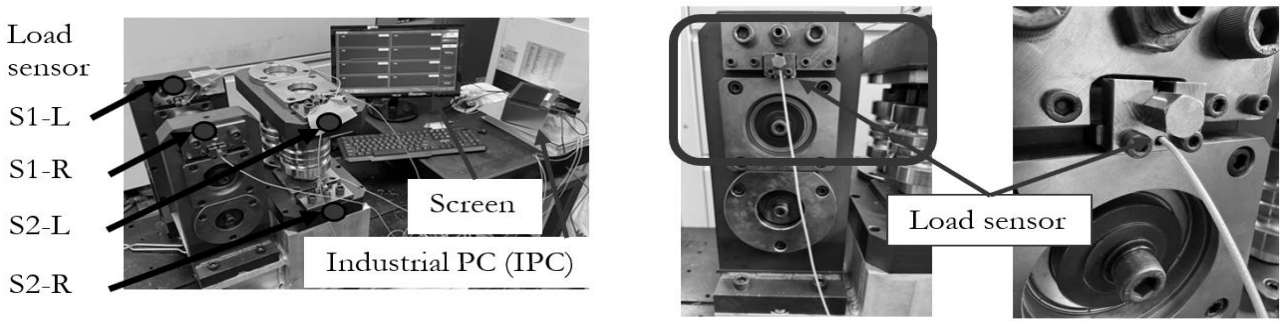

Fig. 11 *Rolling mill load sensor installation and display equipment*

4 Results and discussions

4.1 Forming geometry

In the rolling simulation results, the final cross-sectional geometries of Case 1 (hR_n = 27%) and Case A (hR_n = 24%) are shown in Fig. 12. When hR_n = 27%, the target cross-section is successfully formed. However, in Case A, which simulates poor roll adjustment, a spike phenomenon occurs at S2.

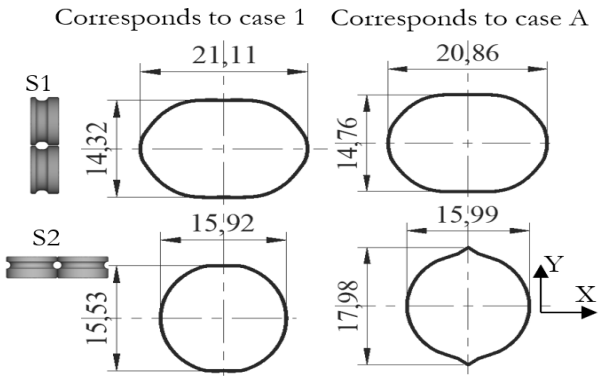

Fig. 12 *Final cross-sectional geometry of FEM simulations for Case 1 and Case A*

In the hot rolling experiment, Fig. 13 presents the forming geometry of Case 1 (wire temperature = 400°C, S1 hR_n = 27%). In Case 2, the wire temperature was adjusted to 350°C, while S1 hR_n remained at 27%, with the forming geometry shown in Fig. 14. Neither Case 1 nor Case 2 exhibited a spike, resulting in the expected forming outcome. However, in Case A, where S1 hR_n was reduced to 24%, a spike was clearly observed (Fig. 15), indicating that the material flow trend during forming aligns with FEM simulation predictions.

The final product dimensions for the three rolling cases are listed in Tab. 5. Compared to FEM predictions, the X-axis width increased by 0.28–0.34 mm, while the Y-axis height decreased by 0.34–0.37 mm, resulting in a more elliptical shape. This discrepancy is primarily attributed to elastic deformation of the roll mold in S2 due to forming loads, as the S2 roll axis is aligned with the Y direction, causing the X-axis dimension to widen.

Additionally, cross-sections from the Case 1 and Case A rolling experiments were extracted (Fig. 16) and compared with the simulated profiles. In Case A, where hR_n was reduced due to poor design, the spike observed in the rolling experiment was even more pronounced than in the numerical simulation. This is attributed to elastic deformation of the roll mold, which increases the roll gap, further exacerbating the spike phenomenon.

Fig. 13 *Case 1: Defect-free product geometry (Stand 1, Section reduction rate 27%, wire temperature 400°C)*

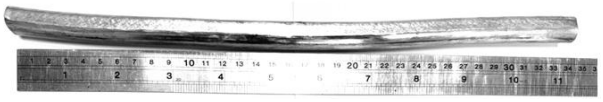

Fig. 14 *Case 2: Defect-free product geometry (Stand 1, Section reduction rate 27%, wire temperature 350°C)*

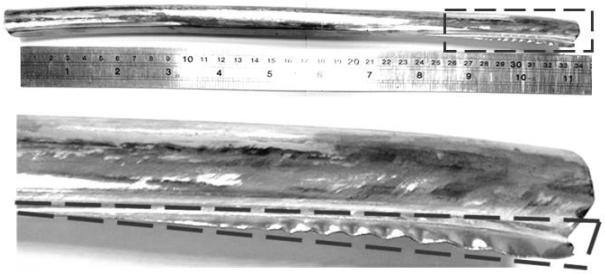

Fig. 15 *Case A: Product with flash defect (Stand 1, Section reduction rate 24%, wire temperature 400°C)*

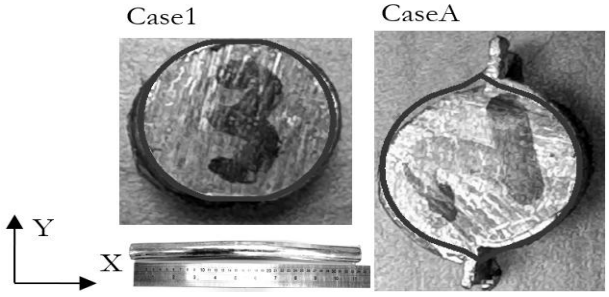

Fig. 16 *Comparison of Experimental and Simulated Cross-Sections for Case 1 and Case A*

Tab. 5 *Measurement of Rolling Product Dimensions*

	hR_n 27%, 400° C (Case1)	hR_n 27%, 350° C (Case2)	hR_n 24%, 400° C (CaseA)
Product X diameter	16.20 mm	16.26 mm	16.28 mm
Product Y diameter	15.19 mm	15.16 mm	spike

4.2 Forming Load

By collecting forming load data from the upper roll sensor, the load curve of Case 1 is shown in Fig. 17. The results indicate that the R-side sensor load is 1.5 to 2 times higher than the L-side sensor load, primarily due to the groove design, where the Rolling side (R) bears a greater load than the Empty side (L).

A comparison between the numerically simulated forming load and the forming load measured in the hot rolling experiment (by summing the R-side and L-side loads) is shown in Fig. 18. The maximum discrepancy between the two is approximately 15%. Additionally, when the wire enters S2, the forming load in S1 increases significantly (by approximately 3 kN, from 25 kN to 28 kN). This occurs because the reduction in cross-sectional area accelerates the forward speed of the wire, making its speed higher than the roll's tangential speed upon entering S2. As a result, the rolls decelerate the wire, inducing axial compression in the longitudinal direction, which leads to an increase in the S1 forming load.

However, this effect was not observed in the numerical simulation, as the speed relationship between S1 and S2 was ideally set in the model.

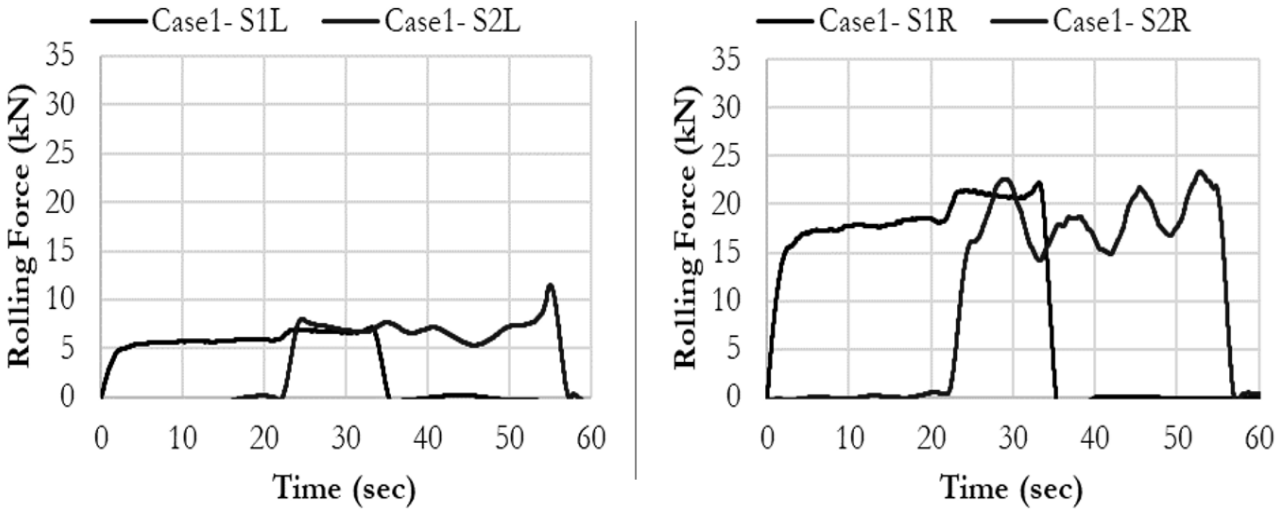

Fig. 17 *Forming Experiment for Case 1, Forming Load Data Collected by Load Sensors*

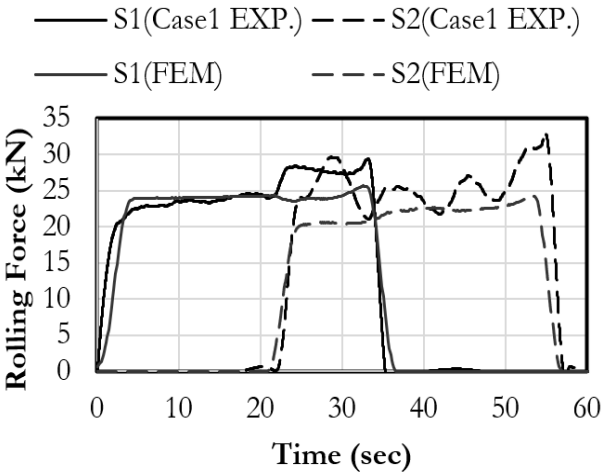

Fig. 18 *Comparison of FEM and rolling experimental loads*

This study compares the forming loads in Case 1 and Case 2, where Case 1 has a wire temperature of 400°C, and Case 2 has a temperature of 350°C. The S1 sensor-collected load data is shown in Fig. 19, revealing that the forming load at 350°C (Case 2) is significantly higher than at 400°C (Case 1). Additionally, the forming time at 350°C is longer, indicating that more sliding occurs during the rolling process.

The S2 sensor-collected load data is shown in Fig. 20. In the S2 load curve, the effect of temperature on forming load is less significant. However, a periodic load fluctuation of approximately 8 seconds is observed. This fluctuation is unrelated to roll speed and may be associated with mechanical springback, although further verification is needed.

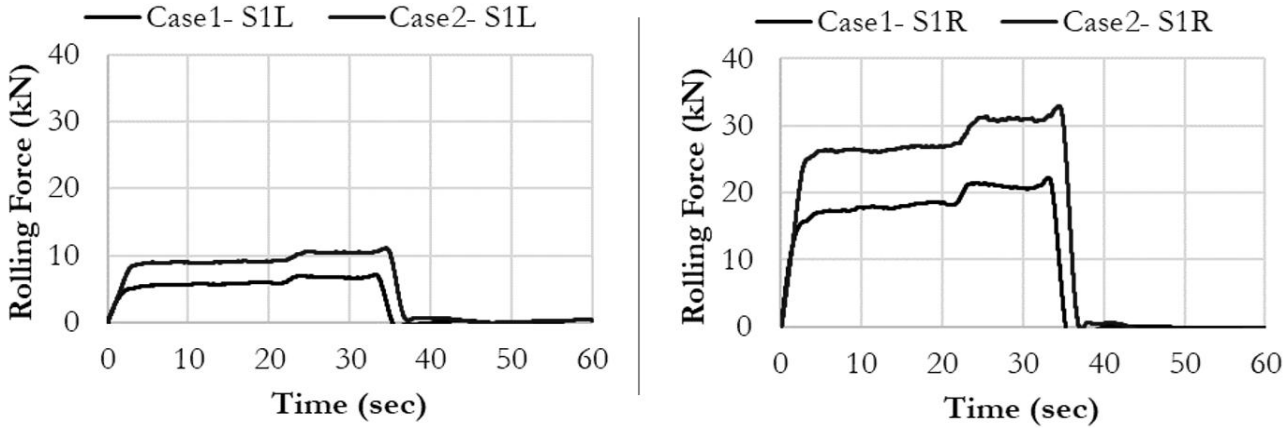

Fig. 19 *Forming load of Stand 1 in Case 1 and 2 experiments*

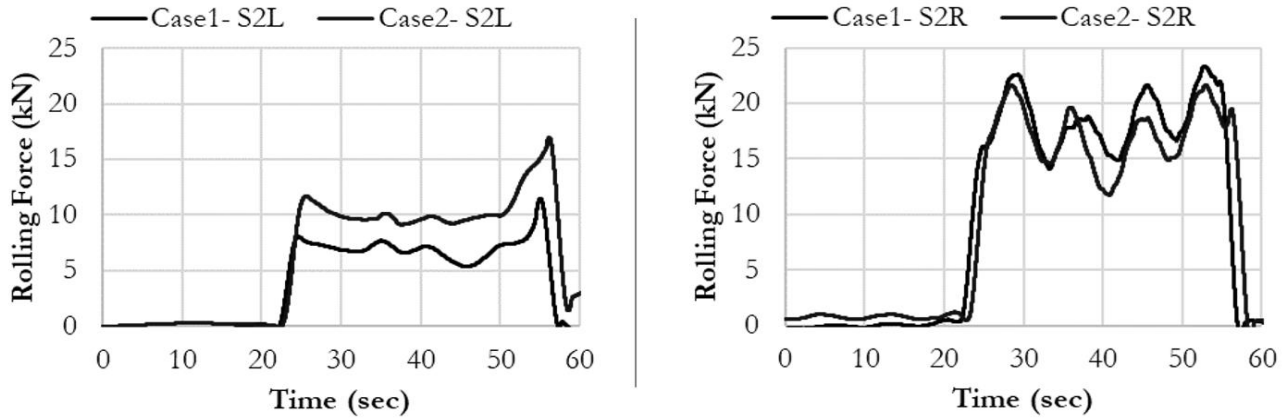

Fig. 20 *Forming load of Stand 2 in Case 1 and 2 experiments*

This study compares the forming loads in Case 1 and Case A, where S1 hR_n is 27% in Case 1 and 24% in Case A, with both cases having the same wire temperature of 400°C. The S1 sensor-collected load data is shown in Fig. 21. The results indicate that in Case A (S1 hR_n = 24%), the forming load does not increase when the wire enters S2. This occurs because, with S1 hR_n reduced to 24%, the wire exit speed at S1 is lower than the S2 roll tangential speed, meaning the wire is not subjected to axial compression, and thus, no increase in S1 forming load is observed.

The S2 sensor-collected load data is shown in Fig. 22. Since the pre-forming hR_n at S1 in Case A is lower, the forming amount at S2 is higher, resulting in a higher S2 forming load compared to Case 1. Additionally, the spike defect in Case A is reflected in a sudden increase in forming load, where the forming load on the rolling side (S2R) increases by approximately 1.7 times, reaching 42 kN.

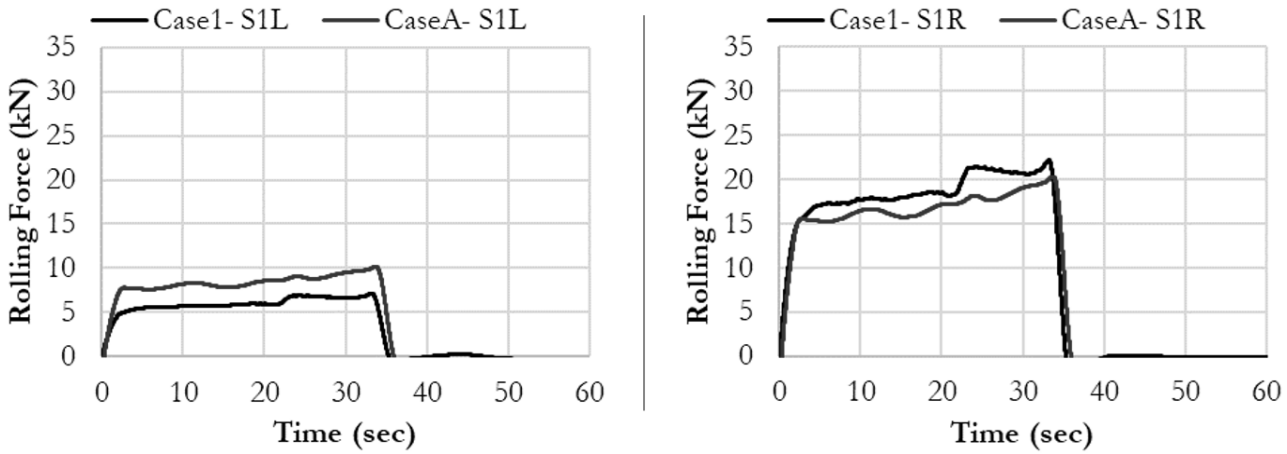

Fig. 21 *Forming load of Stand 1 in Case A and 1 experiments*

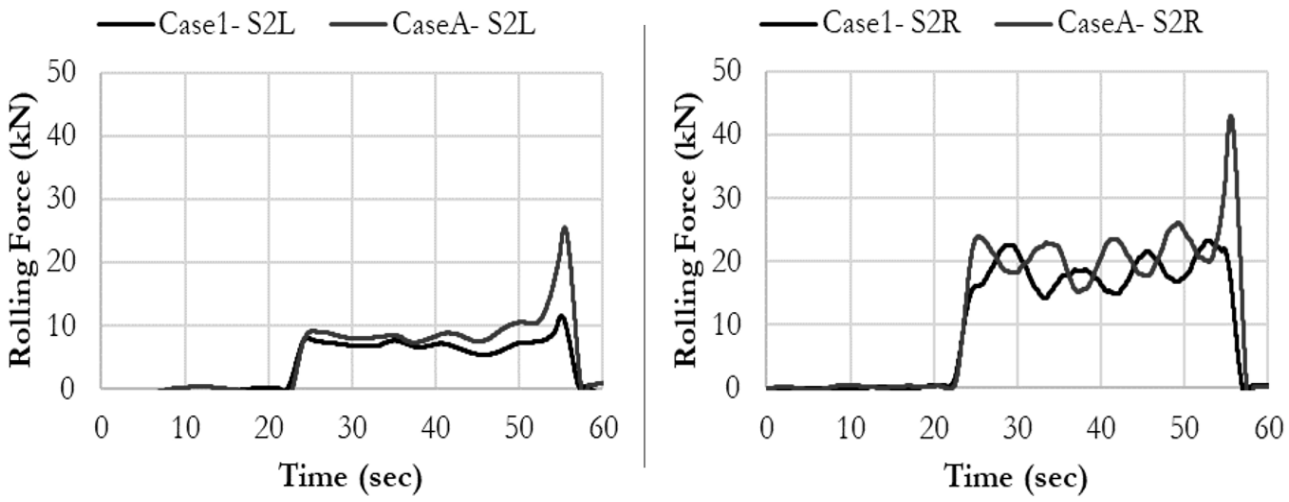

Fig. 22 *Forming load of Stand 2 in Case A and 1 experiments*

4.3 The Distribution of Mechanical Properties in Experimental Results

In this study, Case 1 (without spike defects) and Case A (with spike defects) wires were selected for hardness testing. Test specimens with a height of 15mm were sectioned using a grinding wheel and polished with sandpaper to ensure a smooth and uniform cross-sectional surface.

The actual hardness testing locations are shown in Fig. 23, where each test point was spaced at least two probe diameters apart, and no closer than two probe diameters from the specimen edges, in accordance with standard hardness testing protocols. After obtaining the HRB hardness distribution, the values were converted to equivalent plastic strain using a previously established material model [20], and the results are presented in Tab. 6.

The results indicate that Case 1, formed with the designed reduction rate, exhibits a higher center strain compared to Case A, which exhibited spike defects. In the Y-direction (roll gap area), the strain is notably higher when spike defects are present, indicating localized over-deformation, which aligns with the observed simulation trend in Fig. 24.

To validate the reliability of the simulation, the strain distribution derived from FEM results was compared with the strain converted from hardness data(Fig. 25). The average percentage error between experimental and simulated strain values was found to be 4.6%, demonstrating good agreement and confirming the accuracy of the FEM model in capturing deformation behavior.

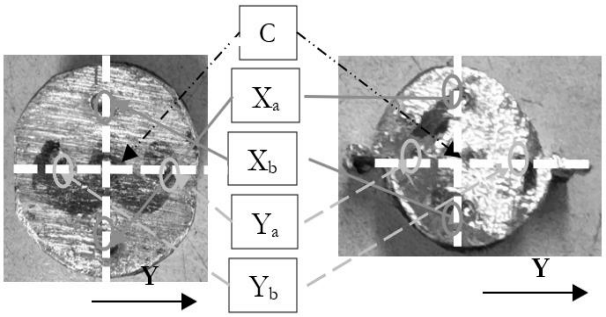

Fig. 23 *The Indentation Locations for HRB Hardness Testing*

Tab. 6 *Strain Distribution Converted from HRB Hardness Testing*

Hardness Measurement Locations	Case 1 Strain, Hardness HRB	Case A Spike Strain, Hardness HRB
C	0.27, 49.9	0.20, 48.1
X_a	0.30, 50.6	0.32, 51.0
X_b	0.36, 51.7	0.27, 49.9
Y_a	0.33, 51.2	0.38, 52.1
Y_b	0.32, 51.0	0.44, 53.0

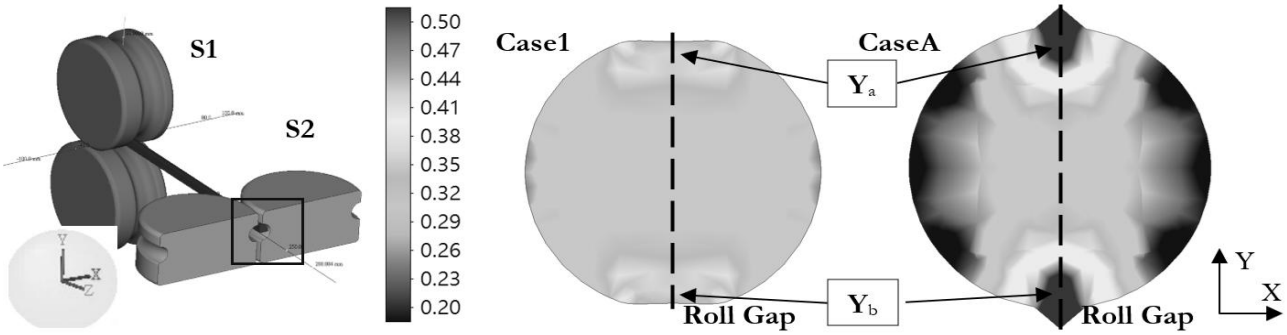

Fig. 24 *Equivalent Strain Distribution of Wire Cross-Section from FEM Simulation*

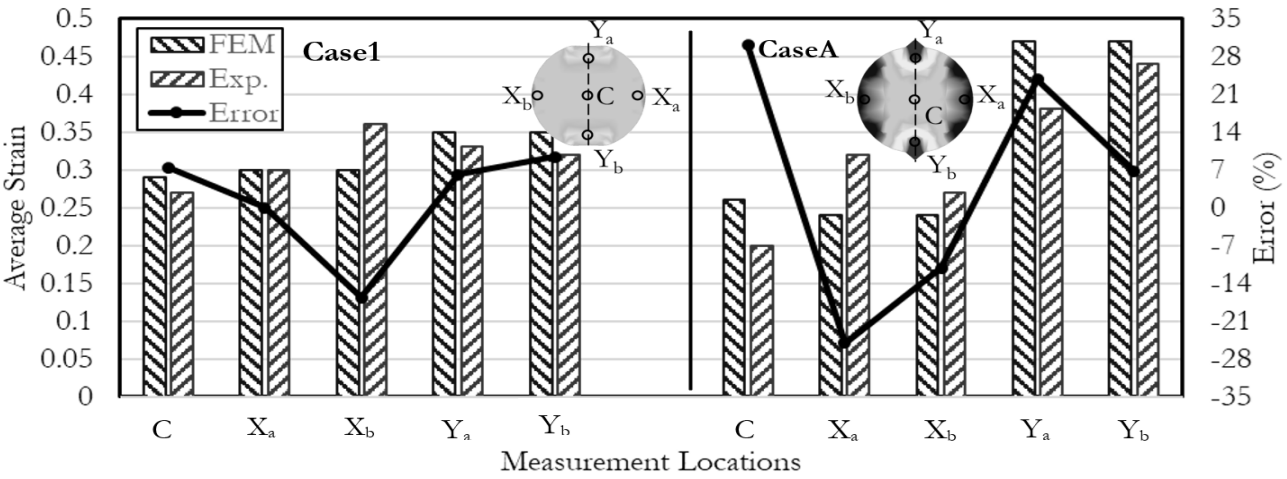

Fig. 25 *Average percentage error between FEM simulation and experimental strain measurements*

4.4 Relationship Between Sensor Load and Uniformity of Finished Product Mechanical Properties

This study evaluates the uniformity of mechanical properties in the final product based on the equivalent strain distribution in the radial (Y) direction (Fig. 24) and uses it as a process quality indicator. As the rolling process progresses, the reduction rate may fluctuate due to roll wear, machine vibration, and other factors. Therefore, real-time process quality assessment can be achieved through forming load measurement.

The forming load reflects process conditions and parameters (Fig. 19–Fig. 22), while process parameters influence the mechanical property distribution of the wire and the occurrence of spike defects (Fig. 23, Fig. 24). This study establishes the correlation between sensor load signals and the target process quality.

Data analysis indicates that the Pearson correlation coefficient is -0.14 for S1 forming load and 0.41 for S2 forming load, suggesting that S2 forming load is more sensitive to process quality variations. Additionally, S1 pre-forming pass hR_n is the key factor affecting process quality distribution, with a Pearson correlation coefficient of 0.91.

To further analyze this relationship, a response surface was developed to correlate target quality, S2R load, and S1 pre-forming hR_n (Fig. 26). The response surface was also visualized in 2D form (Fig. 27), illustrating the relationship between mechanical property uniformity of experimental cases and S2R (Rolling Side) forming load. The experimental results were highly consistent with the regression model established through simulation analysis.

This study successfully predicts the mechanical property distribution of the final product through forming load measurement and process parameter collection during manufacturing.

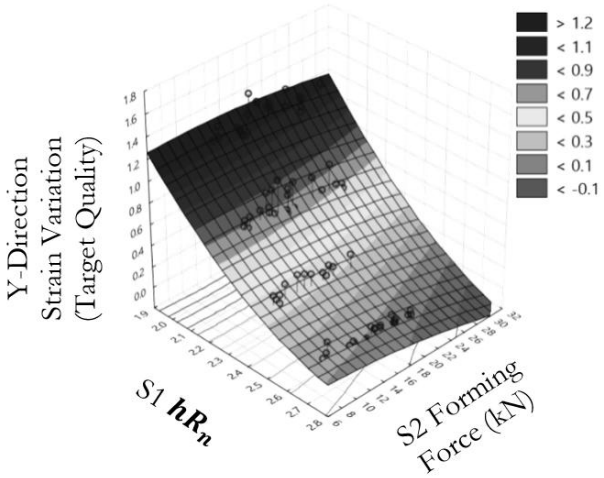

Fig. 26 *Relationship Between S2 Forming Load, S1 hR_n, and Y-Direction Strain Variation (Response Surface)*

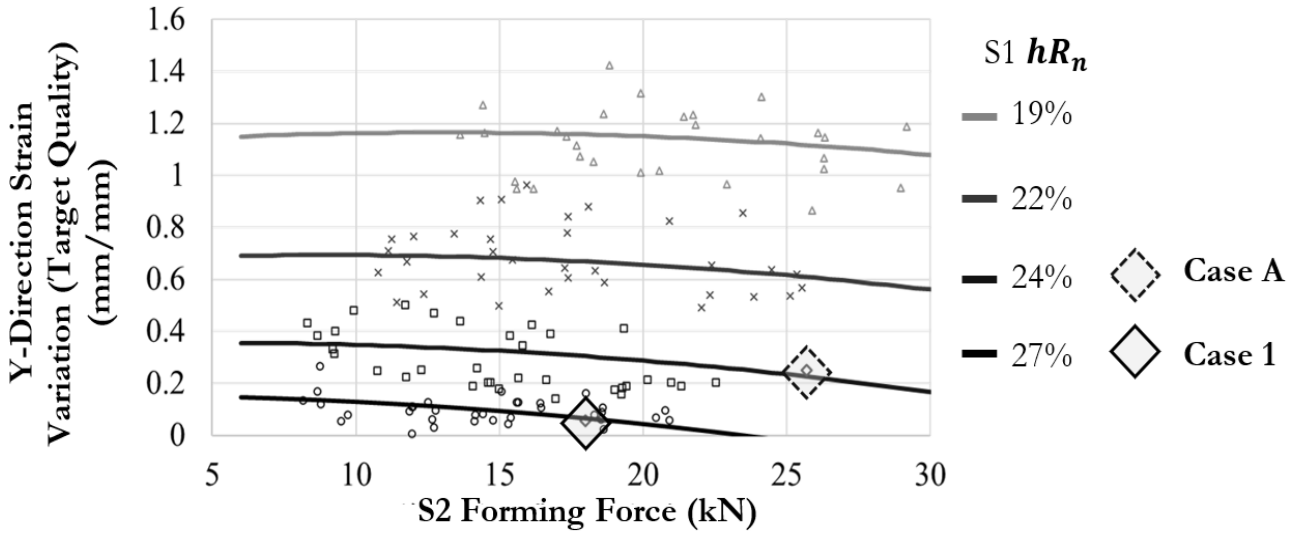

Fig. 27 *Relationship Between S2 Forming Load, S1 hR_n, and Y-Direction Strain Variation (2D− Response Surface)*

5 Conclusions

This study investigates the hot rolling process of EN AW-6061-T6 aluminum alloy wire, focusing on the feasibility and effectiveness of using forming load measurements for process quality evaluation. Forming load data were recorded and analyzed across various conditions to explore their correlation with key process parameters and product quality. The main conclusions are as follows:

- **1. Forming Load Measurement Enables Real-Time Quality Assessment**
  Forming load signals accurately reflect wire temperature changes, multi-pass load balance, and process anomalies due to improper roll design. At a lower temperature of 350 °C, S1 forming load increases by approximately 40% and forming time extends by 3% compared to 400 °C, indicating increased sliding during deformation. The load variation across passes shows that stand one pre-forming section reduction rate (hR_n) directly affects stand two forming load, underscoring its role in load balancing.
- **2. Detection and Impact of the spike Phenomenon**
  Load signals effectively capture the spike phenomenon, caused by improper roll positioning, which results in a sudden surge in S2 forming load on the rolling side (S2R), increasing up to 1.7× (42 kN). This not only indicates mechanical instability but also correlates with reduced strain uniformity in the Y-direction. When stand one section reduction rate is reduced to 24%, the spike becomes more pronounced, while stand one load remains unchanged, suggesting insufficient axial constraint upon entering stand two.
- **3. Pre-Forming Reduction Rate of Stand one Is Critical to Product Uniformity**
  The section reduction rate of stand one is the most influential factor affecting mechanical uniformity and forming load stability. A Pearson correlation coefficient of 0.91 confirms a strong relationship between section reduction rate of stand one and the final product quality. The pre-forming reduction rate also directly affects the right hand side load of stand two and the occurrence of spike defect at stand two.
- **4. Validation and Application Potential of Load-Based Process Monitoring**
  The experimental forming load and strain distribution show good agreement with FEM simulation and statistical modeling results, confirming the reliability of the proposed measurement method. These findings demonstrate that forming load signals can serve as reliable indicators for process adjustment and early-stage defect detection in rolling operations. This approach provides a data-driven basis for quality assurance and offers strong potential for integration with machine learning and smart manufacturing systems.

In conclusion, this study confirms the utility of forming load measurements as a practical and quantitative tool for evaluating process quality, detecting defects, and supporting parameter optimization in hot rolling. Its application offers significant value for quality assurance and future intelligent manufacturing developments.

Acknowledgement

This paper presents the results of project number NSTC 112-2221-E-992-081, funded by the National Science and Technology Council (NSTC) of Taiwan. The support from NSTC has been instrumental in the successful execution of this project, and we would like to express our sincere gratitude for their assistance.

References

[1] BYON, S. M., NA, D. H., LEE, Y. S. (2013). Flow stress equation in range of intermediate strain rates and high temperatures to predict roll force in four-pass continuous rod rolling. In: *Transactions of Non-ferrous Metals Society of China*, Vol. 23, No. 3, pp. 742–748.

[2] BAYOUMI, L. S. (1998). Flow and stresses in round–oval–round roll pass sequence. In: *International Journal of Mechanical Sciences*, Vol. 40, No. 12, pp. 1223–1234.

[3] AKSENOV, S. A., CHUMACHENKO, E. N., LOGASHINA, I. V., KUBINA, T. (2015). Numerical simulation in roll pass design for bar rolling. In: *Metalurgija*, Vol. 54, No. 1, pp. 75–78.

[4] LAMBIASE, F. (2013). Optimization of shape rolling sequences by integrated artificial intelligent techniques. In: *International Journal of Advanced Manufacturing Technology*, Vol. 68, No. 1–4, pp. 443–452.

[5] MINUTOLO, F. C., DURANTE, M., LAMBIASE, F. (2006). Dimensional analysis of a new type of groove for steel rebar rolling. In: *Journal of Materials Processing Technology*, Vol. 175, No. 1–3, pp. 69–76.

[6] SHEU, J. J., HO, C. J., YU, C. H., KAO, C. Y. (2022). High-order groove-shape curve roll design for aluminum alloy 7075 wire rolling. In: *Metals*, Vol. 12, No. 7, pp. 1071.

[7] OVERHAGEN, C., MAUK, P. J. (2014). A new rolling model for three-roll rolling mills. In: *Key Engineering Materials*, Vol. 622–623, pp. 879–886.

[8] CHENOT, J. L., MONTMITONNET, P., BUESSLER, P., FAU, F. (1991). Finite element computation of spread in hot flat and shape rolling with a steady-state approach. In: *Engineering Computations*, Vol. 8, No. 3, pp. 245–255.

[9] BYON, S. M., NA, D. H., LEE, Y. (2009). Effect of roll gap adjustment on exit cross-sectional shape in groove rolling—Experimental and FE analysis. In: *Journal of Materials Processing Technology*, Vol. 209, No. 9, pp. 4465–4470.

[10] BYON, S. M., LEE, Y. (2007). Experimental and semi-analytical study of wear contour of roll groove and its applications to rod mill. In: *ISIJ International*, Vol. 47, No. 7, pp. 1006–1015.

[11] KIM, S. H., IM, Y. T. (1999). A knowledge-based expert system for roll pass and profile design for shape rolling of round and square bars. In: *Journal of Materials Processing Technology*, Vol. 89, pp. 145–151.

[12] LAMBIASE, F., LANGELLA, A. (2009). Automated procedure for roll pass design. In: *Journal of Materials Engineering and Performance*, Vol. 18, No. 3, pp. 263–272.

[13] LI, X., WANG, S., LOHMAR, J., HIRT, G. (2020). Design of caliber rolls incorporating load path dependent damage evolution. In: *Procedia Manufacturing*, Vol. 47, pp. 643–648.

[14] GROCHE, P., HOHMANN, J., ÜBELACKER, D. (2019). Overview and comparison of different sensor positions and measuring methods for the process force measurement in stamping operations. In: *Measurement*, Vol. 135, pp. 122–130.

[15] KIM, S. Y., EBINA, A., SANO, A., KUBOTA, S. (2018). Monitoring of process and tool status in forging process by using bolt type piezo-sensor. In: *Procedia Manufacturing*, Vol. 15, pp. 542–549.

[16] TRAUB, T., GREGÓRIO, M. G., GROCHE, P. (2018). A framework illustrating decision-making in operator assistance systems and its application to a roll forming process. In: *International Journal of Advanced Manufacturing Technology*, Vol. 97, pp. 3701–3710.

[17] TRAUB, T., MÜLLER, C., GROCHE, P. (2019). The perspective of sensor integration and automated decision making in roll forming. In: *AIP Conference Proceedings*, Vol. 2113, No. 1. AIP Publishing.

[18] HWANG, J. K. (2022). Strain and strain rate hardening effects on the macroscopic shear bands and deformation shape of a caliber-rolled wire. In: *Journal of Manufacturing Processes*, Vol. 79, pp. 102–114.

[19] WANG, B., MA, R., ZHOU, J., LI, Z., ZHAO, S., HUANG, X. (2016). Adiabatic shear localization in ultrafine grained 6061 aluminum alloy. In: *Materials Science and Engineering: A*, Vol. 675, pp. 221–227.

[20] ZHANG, Z. J., ZHENG, P. F., CHEN, H., CAI, L. X. (2021). The method for hardness prediction of metal materials based on energy equivalence principle. In: *Engineering Mechanics*, Vol. 38, No. 3, pp. 17–26.

[21] LABER, K. B. (2023). Innovative methodology for physical modelling of multi-pass wire rod rolling with the use of a variable strain scheme. In: *Materials*, Vol. 16, No. 2, pp. 578.

[22] HO, C. J., YU, C. H., KAO, C. Y., SHEU, J. J. (2021). Process design and finite element analysis of multi-station two-roller cassette hot rolling for aluminum alloy 6061 wire. In: *Journal of Physics: Conference Series*, Vol. 2020, No. 1, pp. 012036.

[23] BONTCHEVA, N., PETZOV, G. (2005). Total simulation model of the thermo-mechanical process in shape rolling of steel rods. In: *Computational Materials Science*, Vol. 34, No. 4, pp. 377–388.

[24] SYGUT, P., LABER, K., BORKOWSKI, S. (2012). Investigation of the non-uniform temperature distribution on the metallic charge length during round bars rolling process. In: *Manufacturing Technology*, Vol. 12, No. 13, pp. 260–263.

[25] ZHANG, D. W., ZHAO, S. D. (2018). Influences of friction condition and end shape of billet on convex at root of spline by rolling with round dies. In: *Manufacturing Technology*, Vol. 18, No. 1, pp. 165–169.

[26] SAKHAEI, A. H., SALIMI, M., KADKHODAEI, M. (2013). New multi-pass hot channel section rolling design by the finite element method. In: *Journal of Mechanical Engineering Science*, Vol. 227, No. 12, pp. 2742–2750.

[27] ZHAO, X., CHEN, L., HE, K., WU, N., ZENG, J. (2019). Effect of contact heat transfer on hot rolling of aluminum alloy. In: *Procedia Manufacturing*, Vol. 37, pp. 91–96.